



Asian Journal of Chemistry;


Vol. 37, No. 12 (2025), 3086-3092

ASIAN JOURNAL OF CHEMISTRY

<https://doi.org/10.14233/ajchem.2025.34737>



Sunlight Tempted Photodegradation of Methylene Blue using Cerium Doped La_2O_3 Photocatalyst

ROSHAN REKHATE and NITIN BANSOD^{*,}

Nanotechnology Research Laboratory, Department of Chemistry, Shri Shivaji Science College, Amravati-444603, India

*Corresponding author: E-mail: nbansod15@gmail.com

Received: 20 August 2025

Accepted: 16 October 2025

Published online: 30 November 2025

AJC-22199

In this study, we report the synthesis of pristine and cerium (Ce)-doped lanthanum oxide (La_2O_3) nanomaterials *via* a sol-gel combustion method and their application as efficient photocatalysts for the degradation of methylene blue (MB) dye under natural sunlight. Structural characterization by X-ray diffraction (XRD) confirmed the formation of hexagonal La_2O_3 , with slight peak shifts observed upon Ce doping due to nanoscale lattice strain. Morphological analyses using SEM and TEM revealed that Ce doping induced the formation of a 3D network-like structure, enhancing surface area and active sites for pollutant adsorption. UV-visible spectroscopy demonstrated a reduction in the band gap from 5.56 eV for pristine La_2O_3 to 5.27 eV for 9% Ce-doped La_2O_3 , facilitating improved visible-light absorption and reduced electron-hole recombination. Fourier-transform infrared (FTIR) and energy-dispersive X-ray (EDAX) analyses further confirmed the successful incorporation of Ce into the La_2O_3 matrix without impurities. Photocatalytic experiments showed that 7% Ce-doped La_2O_3 achieved the highest degradation efficiency of ~94% for MB dye within 90 min, outperforming pristine La_2O_3 (78%) and lower doped variants. The enhanced performance is attributed to band gap narrowing, effective charge carrier separation, and the unique network morphology of the doped nanomaterial. This study highlights the potential of Ce-doped La_2O_3 as a robust, visible-light-active photocatalyst for sustainable wastewater treatment applications.

Keywords: Photocatalyst, Methylene blue, Cerium doped lanthanum oxide.

INTRODUCTION

The rapid pace of industrialization and urban development is depleting natural resources and worsening water pollution across agricultural and domestic sectors. Industrial effluents rich in organic and inorganic pollutants present a growing hazard to human well-being [1,2]. The literature clearly suggests that more than one billion people from developing countries are in a risk of water contaminant impurity caused due to several pollutants [3,4]. These pollutants include dyes, organic byproducts, petroleum/oil wastes being discharged from several chemical, fertilizer, textile industries, *etc.* [4,5]. Various physico-chemical methods *viz.* filtration, adsorption, reverse osmosis, coagulation and chemical precipitation are conventionally available for the treatment of wastewater [6].

In recent years, semiconductor based photocatalysis as one of the promoted oxidation processes has been emerged as a challenging and effective technique for wastewater treatment which is capable of transforming organic pollutants into CO_2 , water and inorganic byproducts [7-12]. Photocatalysis employ a photocatalysts with tuneable band gap which can

be further utilized for clampdown of e^-/h^+ recombination and effective absorption of visible light [13,14]. Conventional photocatalysts with wide band gap experiences limitations in certain cases. To overcome this drawback, non-conventional photocatalysts modified with carbonaceous support *viz.* graphene oxide (GO), nanotubes, graphitic carbon nitride or MXenes are used which helps to reduce e^-/h^+ pair recombination [15]. Band gap of pristine metal oxide can also be tuned to visible region by doping with several elements *viz.* Ag, Pt, Au, Cu *etc.* [16,17]. Since, approximately 42% part of solar spectrum comprises of visible light and a few (~ 4%) comprises of UV light, the improvement of visible light active photocatalysts is of primary research need.

Nanocomposites (NCs) incorporating metal oxide nanoparticles (NPs) have attracted growing attention across various scientific fields due to their favourable properties, including low cost, non-toxicity and sustainability [18,19]. More than, these metal oxide nanoparticles possess advantageous features including exceeding surface area, remarkable electrical conductivity and stout chemical consistency [20].

This is an open access journal, and articles are distributed under the terms of the Attribution 4.0 International (CC BY 4.0) License. This license lets others distribute, remix, tweak, and build upon your work, even commercially, as long as they credit the author for the original creation. You must give appropriate credit, provide a link to the license, and indicate if changes were made.

Recently, lanthanum oxide (La_2O_3), has garnered increased attention as a promising photocatalyst owing to its unique physical characteristics including tuneable opto-electronic characteristics and wider bandgap. Since, lanthanum is the only rare earth element which lacks $4f$ -electrons and resembles the behaviour of xenon [21]. Rare earth elements have characters of partially filled $4f$ -subshell and vacant $5d$ -subshell associated with rare earth elements facilitates the effective charge carrier separation and pave the path towards their use as a promising photocatalyst. Therefore, La_2O_3 , in its powdered form demonstrates several characteristics such as stability, good thermal flexibility, robust mechanical properties and light emitting characteristics [22]. Owing to incomparable characteristics of La_2O_3 , it has demonstrated its applications in diverse fields, including gas sensing [23], protective coating material [24], thermoelectric devices [25], as a photocatalyst [26], as an electrode material in solid oxide fuel cells [27], micro-electronics [28], biomedical applications [29], *etc.* Moreover, the special opto-electronic characteristics, tunable bandgap, ample dielectric constant and the lower-most lattice energy associated with La_2O_3 has proved to be favourable for its use as a photocatalyst for wastewater treatment [30].

In this investigation, we have successfully employed a sol-gel method for the synthesis of crystalline cerium-doped La_2O_3 nanomaterial and to explore its application in wastewater treatment for degradation of methylene blue (MB) dye. A doping strategy was used to tune the bandgap of La_2O_3 by using cerium. Successful synthesis of Ce doped La_2O_3 using sol-gel technique and its application in wastewater treatment embraces the novelty of current study.

EXPERIMENTAL

All chemicals were purchased from Sigma-Aldrich and used without further purification. The analytical grade lanthanum nitrate hexahydrate ($\geq 99\%$), cerium nitrate pentahydrate (99.9%), citric acid and ammonia solution were used as starting materials. Methylene blue was used as a source of model dye contaminant.

Synthesis of pristine and Ce-doped La_2O_3 photocatalysts: For synthesis of pristine and Ce-doped La_2O_3 nanomaterials a sol-gel combustion method was used. During synthesis, $\text{La}(\text{NO}_3)_3 \cdot 6\text{H}_2\text{O}$, $\text{Ce}(\text{NO}_3)_3 \cdot 5\text{H}_2\text{O}$ and $\text{C}_6\text{H}_8\text{O}_7 \cdot \text{H}_2\text{O}$ (citric acid) were used as the precursor material. Typically, in sol-gel synthesis method, citric acid acts as a reducing agent, while metal nitrates act as an oxidizing agent. Citric acid also serves as an organic fuel, providing a platform for redox reactions to take place between the reactants during combustion [31,32]. Metal nitrates were weighed stoichiometrically and dissolved in minimal deionized water to obtain clear solutions, which were then mixed with an aqueous citric acid solution under stirring for 30 min, maintaining a constant molar ratio. The mixture was further stirred for 2 h at neutral pH using NH_3 solution, followed by hydrothermal treatment in an autoclave at 20 atm for 12 h to form solid particles. The resulting solids were collected and calcined to obtain the final nanomaterials.

Material characterization: Structural characterization of as-synthesized material was done using the Shimadzu XRD-6100 diffractometer with radiation source $\text{CuK}\alpha$ 0.15402 nm in

the range of 20 – 80° . The morphological characterization was done using SEM analysis equipped with EDAX (Zeiss Gemini 500 FE-SEM) as well as with TEM techniques. Spectral studies for functional group identification were done through the Shimadzu IR Affinity-1S FTIR spectrometer in the range of 4000 – 400 cm^{-1} . Optical studies were done to record the UV-Visible spectra using Cary 60 spectrophotometer to study pollutant degradation through absorption behaviour.

Photocatalytic experiments: The as-synthesized La_2O_3 and Ce-doped La_2O_3 photocatalyst were further tested for their photocatalytic activities by degrading methylene blue (MB) dye as a model organic pollutant. During photocatalytic experiments, approximately 25 mg of photocatalyst was suspended in 100 ppm solution of MB dye and the solution was kept in dark for 1 h in order to achieve the absorption-desorption equilibria. After 1 h, the solution was exposed to natural sunlight under constant agitation using magnetic stirrer. During photocatalytic experiments, the aliquots of solution were withdrawn at regulated intervals of 10 min and were subjected to UV-visible spectrophotometer after centrifugation. The extent of MB dye photodegradation was monitored by observing the time dependent UV-visible spectrum of residual MB dye.

Percentage degradation was determined by the following relation:

$$\text{Degradation (\%)} = \frac{C_i}{C_o} \times 100$$

where C_i is the concentration at time t whereas C_o is the initial concentration.

RESULTS AND DISCUSSION

XRD studies: The as-synthesized nanomaterials *i.e.* pristine and Ce-doped La_2O_3 were examined for their structural confirmation using powder X-ray diffractometer and the results are depicted in Fig. 1a-b. X-ray diffraction (XRD) analysis in the range of 20 – 80° has confirmed the structure of synthesized nanoparticles of pure hexagonal La_2O_3 with space group $P6_3/mmc$ having lattice parameters as $a = 3.9373\text{ \AA}$, $b = 3.9373\text{ \AA}$ and $c = 6.1299\text{ \AA}$, which in accordance with the standard card (JCPDS no. 01-074-2430) [33]. The reflections appearing at 2θ angles of 29.9° , 39.5° , 46.0° and 52.1° can be indexed to (101), (102), (110) and (103) planes as per indexed with card. Moreover, the diffraction peak at 44.8° corresponds to the hexagonal $\text{La}_2\text{O}_2\text{CO}_3$ phase (JCPDS 84-1963), formed through partial conversion of La_2O_3 during calcination. Rare-earth doping typically induces peak broadening due to nano-scale confinement and internal stresses. As evident from Fig. 1b, these tensile or compressive stresses cause a slight shift in the diffraction peaks [34].

UV-visible studies: The optical characteristics of cerium-doped La_2O_3 samples were further studied by observing their UV-visible absorption recorded in a wavelength range 200 – 800 nm . The spectra were recorded after sonicating the solution of 0.1 g sample in 50 mL of water. The UV-visible absorption spectra of as-synthesized Ce-doped La_2O_3 samples is depicted in Fig. 2a-b. It is observed that 3%, 5%, 7% and 9% Ce-doped La_2O_3 samples exhibit a characteristic absorption peak at 223, 231, 228 and 235 nm, respectively. The calculated band gap

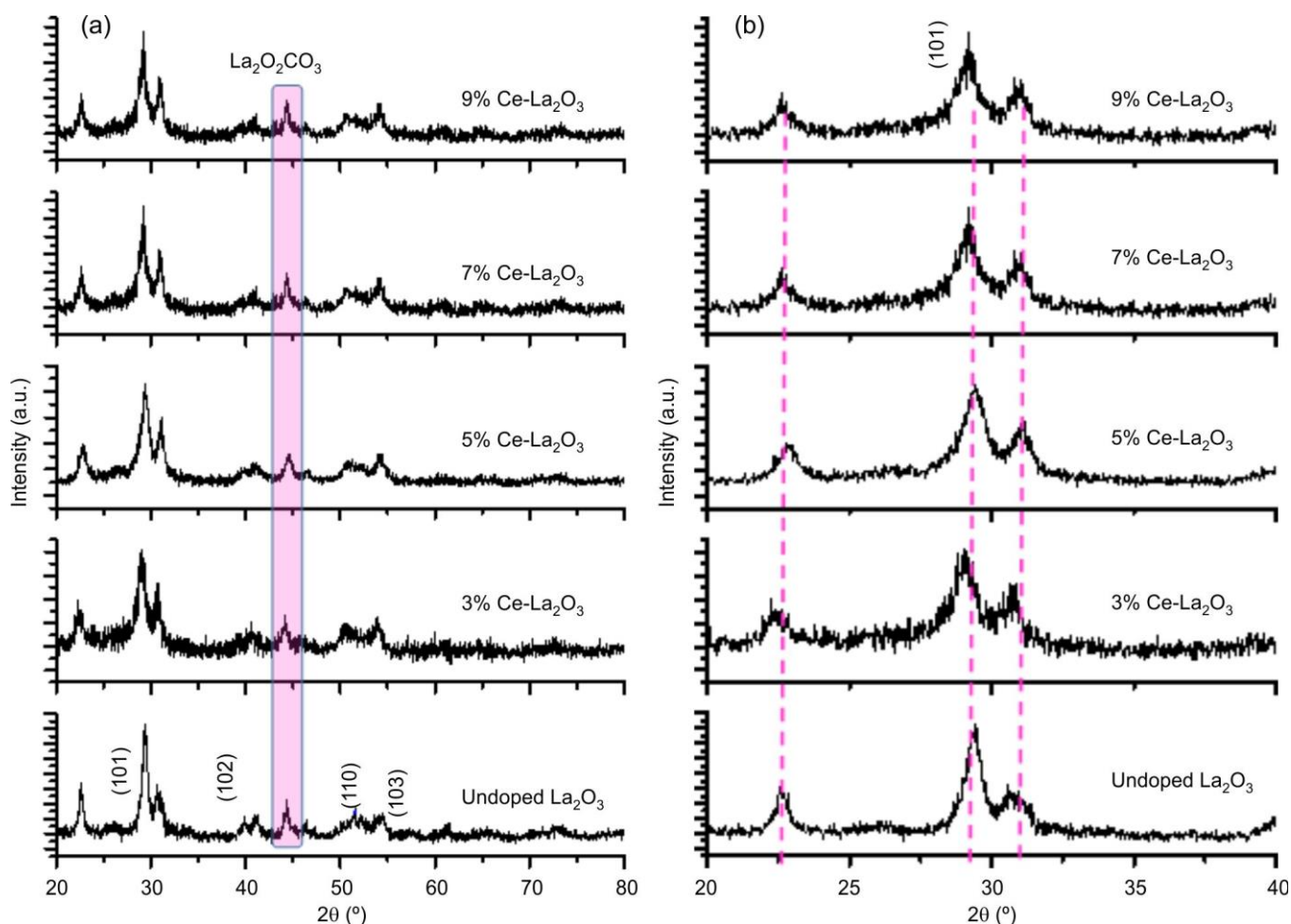


Fig. 1. (a) XRD of pristine La_2O_3 and representative Ce doped La_2O_3 samples, (b) peak shifting

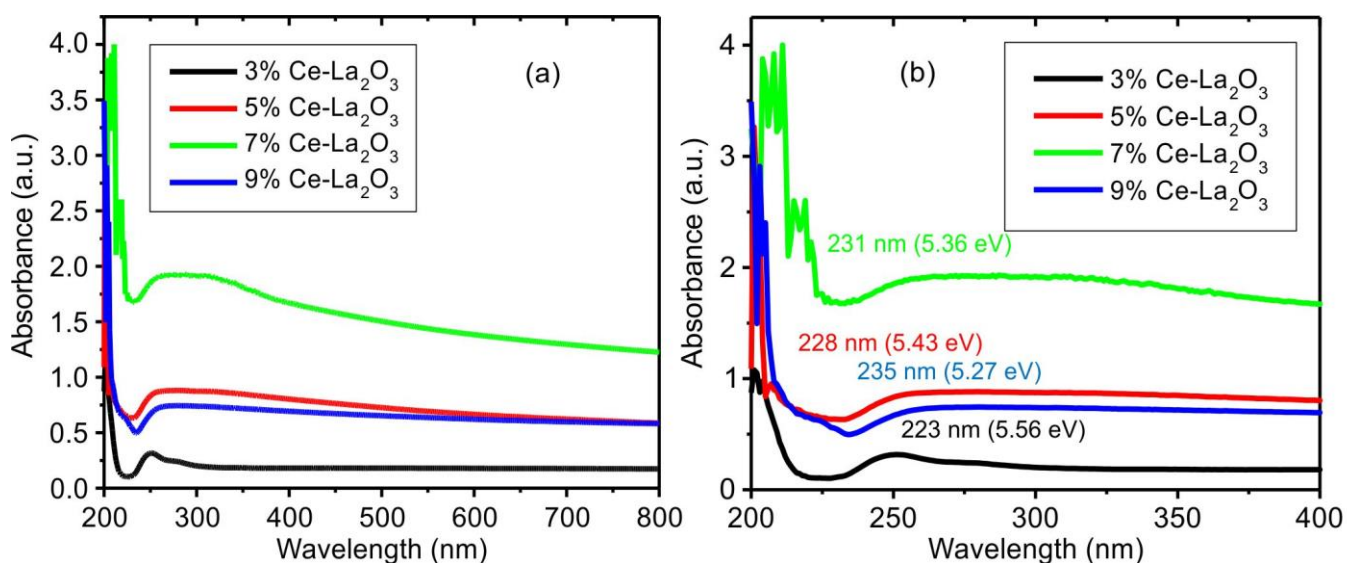


Fig. 2. (a) UV-visible absorption spectra of as-synthesized Ce doped La_2O_3 samples (b) enlarged view of absorption peaks

energies corresponding to these absorptions are 5.56, 5.36, 5.43 and 5.27 eV, respectively for 3%, 5%, 7% and 9% Ce-doped La_2O_3 samples. The reduction in band gap resulting from Ce incorporation is consistent with the lattice distortions and peak shifts identified in the XRD results.

FTIR studies: The as-synthesized pristine and Ce-doped La_2O_3 samples were further studied for the functionalities and bond detection using FTIR spectroscopy. The FTIR spectra were recorded over the wavelength range $4000\text{--}400\text{ cm}^{-1}$ and the results are depicted in Fig. 3a-b. Broad absorption bands

appearing at $3500\text{--}3400\text{ cm}^{-1}$ (in broad range from 3481 cm^{-1} in La_2O_3 to 3456 cm^{-1} in 7% Ce-doped La_2O_3) can be ascribed to stretching vibrations of O-H due to the presence of water [35]. The peak appearing at 866 , 1075 and 1370 cm^{-1} further confirmed La-O bond stretching vibrations [36,37].

SEM-EDAX studies: The morphological investigations of the as-synthesized samples were further done by SEM analysis equipped with EDAX. The allied results are depicted in Fig. 4a-m below. The low and high magnification images of pristine La_2O_3 are depicted in Fig. 4a-b. SEM results suggest the fine particle morphology of synthesized sample which ranges in between $10\text{--}50\text{ nm}$. As can be seen from the elemental mapping images of undoped La_2O_3 (Fig. 4c-e), the samples are purely consisting of La and O and are free from any other impurities which is further evidenced by the corresponding EDAX graph as depicted in Fig. 4f. For morphological investigation of Ce-doped La_2O_3 samples, a representative 7% Ce-doped sample was employed and the results are shown in Fig. 4g-m. As can be seen from the SEM images shown in Fig. g-h, the doping of La_2O_3 with Ce has significant influence on the morphology. Specifically, the particle like nature has been changed to agglomerated structures with slight increase in particle size. Further, the elemental mapping images and the corresponding EDAX graph suggests that the dopant element Ce is uniformly distributed in the La_2O_3 matrix and sample is composed of La, Ce and O elements only. Also,

there are no any impurity peaks observed in the graph suggesting the successful synthesis of Ce-doped La_2O_3 sample.

TEM studies: The morphological investigation of as-synthesized pristine and a representative 7% Ce-doped La_2O_3 samples were done by TEM analysis equipped with SEAD and the results are depicted in Fig. 4a-h. Low and high magnification images of pristine La_2O_3 (Fig. 4a-c) depicts that pristine La_2O_3 exhibits a distinct rectangular morphology and is uniformly grown. For Ce-doped La_2O_3 sample, it seems to be formation of a 3D network-like structure with these rectangular particles as a unit building block. These network like structure has provided any groves which might further be useful for trapping organic wastewater contaminants from photodegradation application. Further, the SAED analysis uncovered discrete rings consistent to several planes, *i.e.*, (222), (012), (111) and (112), in case of both the pristine and Ce-doped La_2O_3 samples, Fig. 5d&h. The TEM images along with SEAD analysis further confirms the formation of well-crystallized pristine as well as Ce-doped La_2O_3 material, which is in consistent with the findings from XRD data.

Photocatalytic degradation of methylene blue (MB)

dye: The photocatalytic efficiency of as-synthesized pristine and Ce-doped La_2O_3 was further tested by using a MB as a model dye contaminant. The photocatalytic degradation of MB dye was performed for a period of 100 min under natural sunlight. In general, photocatalytic degradation of any organic

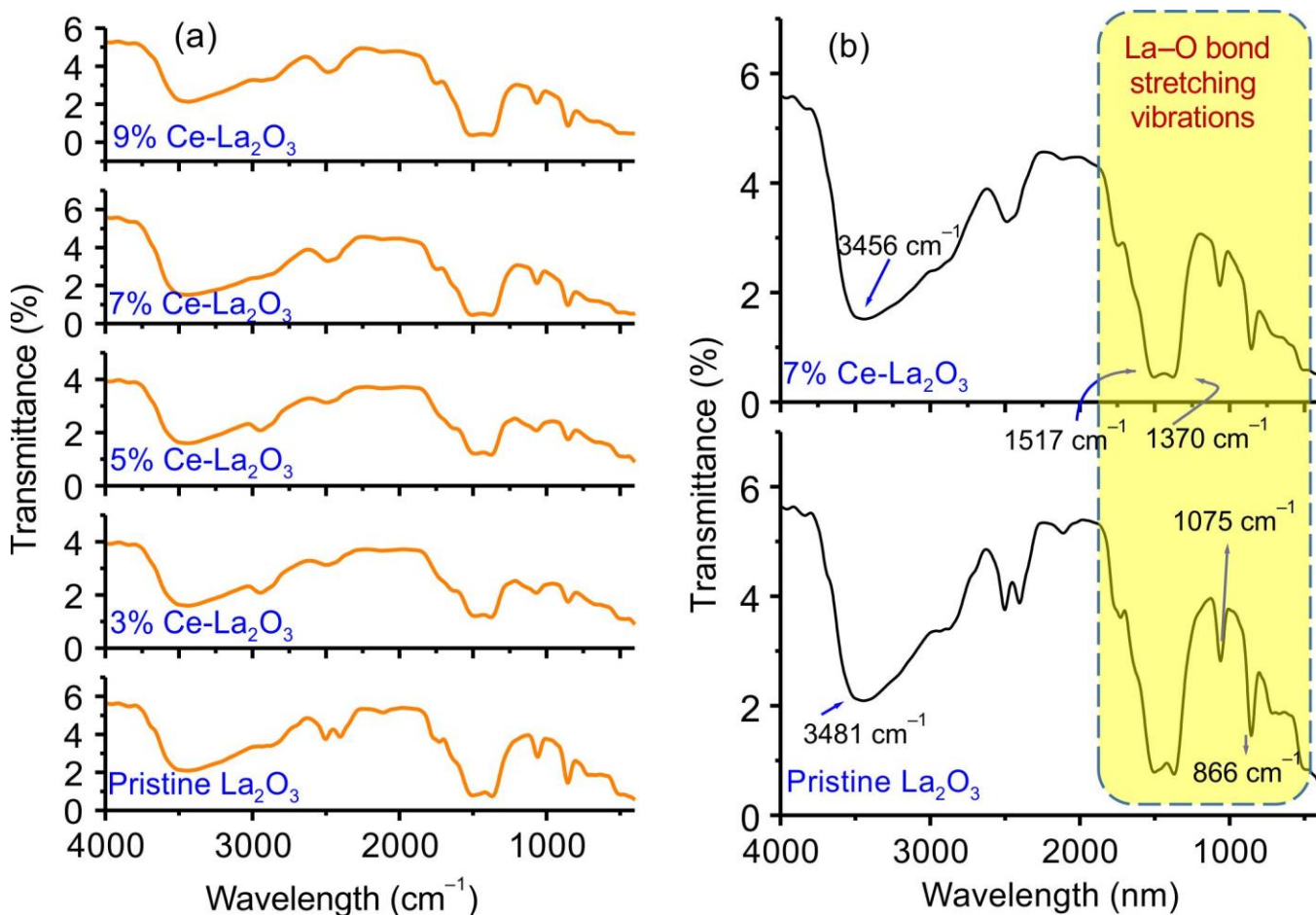


Fig. 3. (a) FTIR spectra of as-synthesized pristine and Ce doped La_2O_3 samples (b) High magnification view of absorption peaks

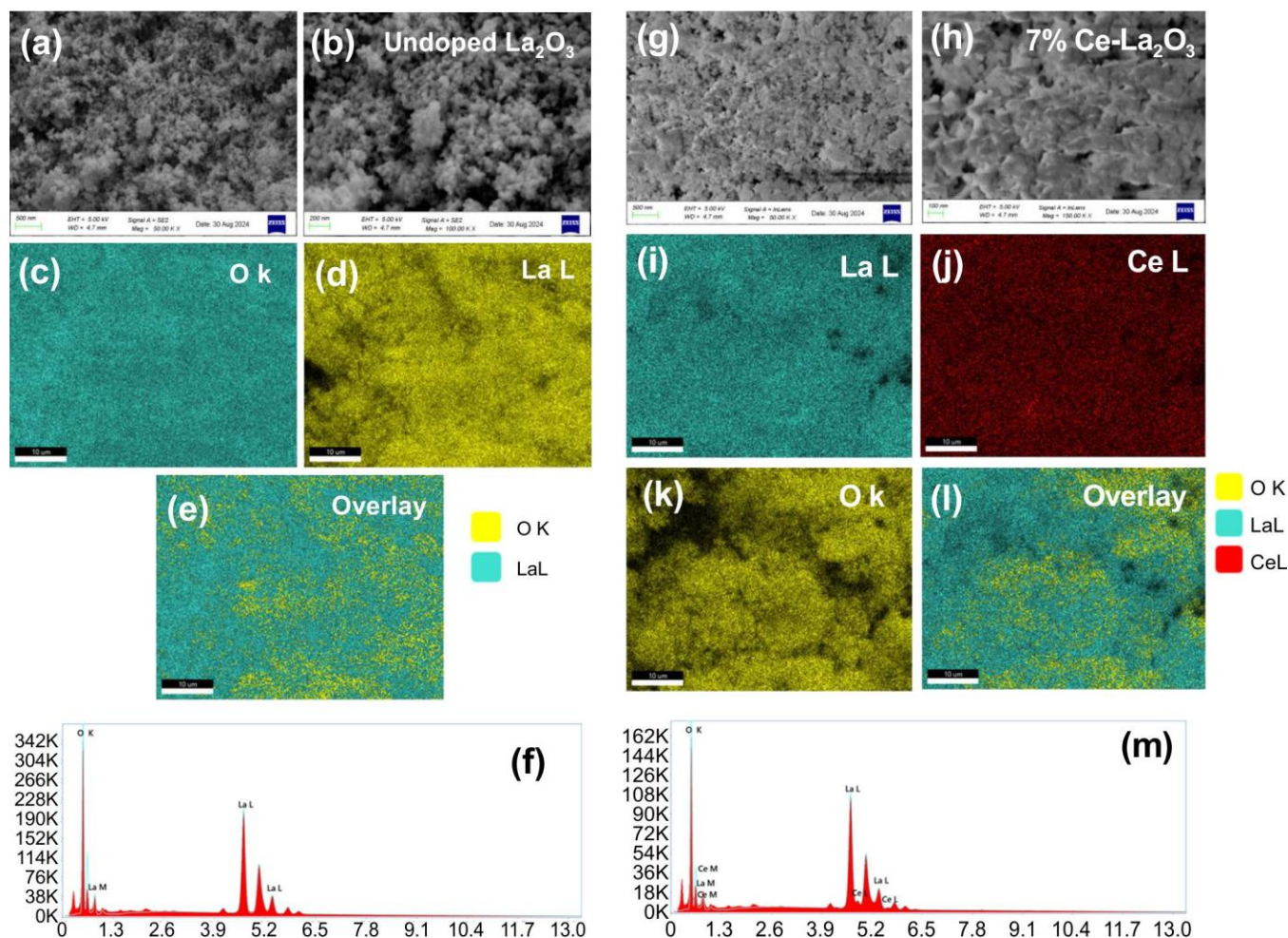


Fig. 4. (a,b & g,h) Low and high magnification SEM images of undoped and a representative 7% Ce doped La_2O_3 samples (c-e & i-l) corresponding images of elemental colour mapping; (f & m) shows the EDAX spectra of the samples

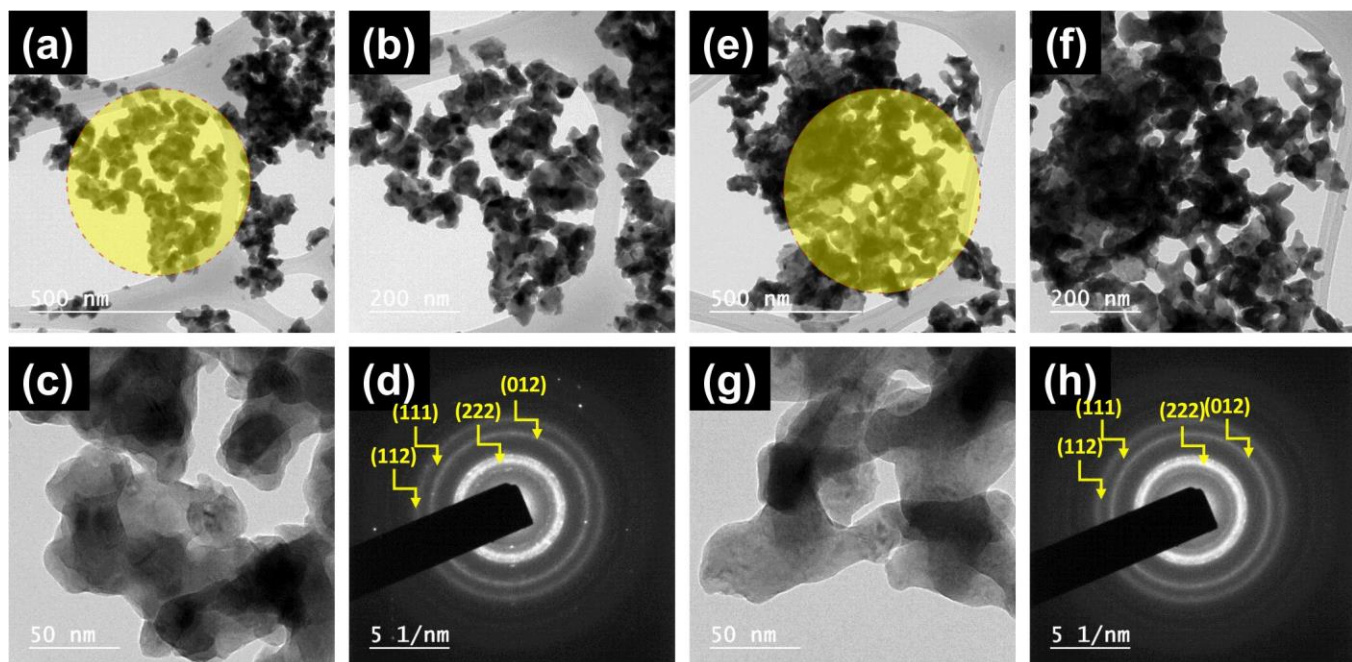


Fig. 5. Low and high magnification images of (a-c) pristine and (e-g) representative 7% Ce doped La_2O_3 samples (d & h) corresponding SAED patterns

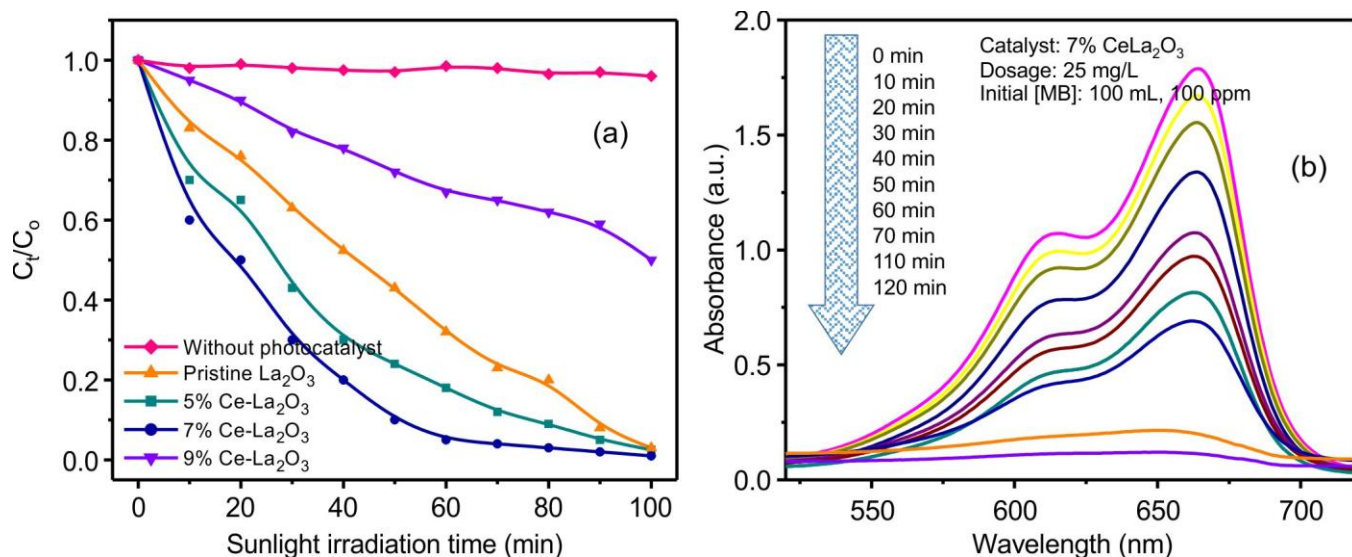


Fig. 6. (a) Time dependent degradation rates of MB dye over as-synthesized pristine and Ce-doped La_2O_3 samples, (b) Time dependent absorption spectra of MB dye during photodegradation using 7% Ce- La_2O_3 photocatalyst

contaminant in presence of a photocatalyst irradiated by a light source proceeds *via* three steps, out of which first step comprises of energy harvesting in the form of photons by the photocatalyst. In second step, there is a generation of electron hole pairs and their transition. Third step involves, the series of redox reactions at the surface of photocatalyst. These redox reactions are mainly responsible for breakdown of target contaminant molecules. As evident from the UV-visible analysis of as-synthesized photocatalysts, after doping La_2O_3 with cerium, a gradual decrease in band gap was observed which mainly be resulted in reduction of charge-carrier recombination level. Abundant availability of electrons for oxygen reduction at the active sites eventually retard the electron hole recombination rate and thus the band gap narrowing occurs [38].

The photocatalytic degradation performance of pristine and Ce-doped La_2O_3 toward MB dye is shown in Fig. 6a. Under sunlight irradiation, pristine La_2O_3 achieved ~78% degradation within 90 min, while 5% Ce-doped La_2O_3 showed an enhanced efficiency of ~83%. The blank experiment confirmed minimal degradation (3-4%) in the absence of a photocatalyst. The highest efficiency was obtained with 7% Ce-doped La_2O_3 , which degraded ~94% of MB within the same period. This enhanced activity is further supported by the time-dependent absorption spectra as shown in Fig. 6b. Overall, MB degradation increased with Ce content up to 7%, beyond which the activity declined. The superior performance of the 7% Ce-doped sample is attributed to reduced electron-hole recombination due to band-gap narrowing, along with its larger surface area and network-like morphology. Based on the photocatalytic experiment results, a possible mechanism for effective photodegradation is proposed and is schematically represented in Fig. 7.

The photocatalytic degradation of MB dye over as-synthesized photocatalyst encompasses a series of complex reactions, which predominantly includes adsorption-desorption, electron-hole formation and recombination and further redox reactions. Initially, upon sunlight irradiation the photocatalyst material absorbs the energy equal to or more than the bandgap (E_g) of

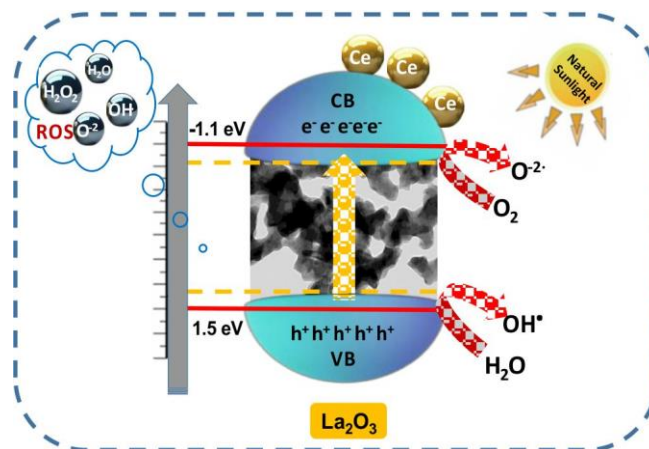


Fig. 7. Schematic diagram representing the possible photodegradation of methylene blue dye degradation over as-synthesized Ce doped La_2O_3 photocatalyst

photocatalyst material leading to subsequent photoexcitation. These photons excite valence band (VB) electrons to conduction band (CB) leaving behind the holes in the VB, resulting in the establishment of e^-/h^+ pairs. The photo-induced electrons generate superoxide radical $\text{O}_2^{\cdot-}$ by reacting with oxygen, which further reacting with water generates the oxidizing species such as hydroxyl radicals. Finally, the oxidation of organic molecules harvests CO_2 and H_2O .

Conclusion

A cost-effective, facile sol-gel combustion method was employed for the synthesis of pristine and Ce-doped La_2O_3 nanoparticles. The XRD spectra confirmed the presence of hexagonal La_2O_3 with space group $P63/mmc$ having lattice parameters as $a = 3.9373\text{\AA}$, $b = 3.9373\text{\AA}$ and $c = 6.1299\text{\AA}$. The UV-visible absorption spectroscopy reveals the band-gap narrowing upon Ce doping. TEM revealed the network-like morphology of Ce doped La_2O_3 synthesized using sol-gel technique. The photocatalytic degradation of MB dye was monitored to evaluate the photocatalytic efficiency of Ce

doped La₂O₃, 7% Ce-La₂O₃ demonstrated the best photocatalytic efficiency of 94% photodegradation within 90 min.

ACKNOWLEDGEMENTS

The authors thank the Principal, Shri Shivaji Science College, Amravati for providing the research facilities to carry out experimental work. The authors also gratefully acknowledge Sprint Lab, Mumbai for providing instrumental facilities like SEM, EDAX, TEM as well as Shri Shivaji Science College, Amravati for providing FTIR spectra, UV Visible spectra and XRD analysis.

CONFLICT OF INTEREST

The authors declare that there is no conflict of interests regarding the publication of this article.

REFERENCES

1. K. Ghorai, A. Panda, A. Hossain, M. Bhattacharjee, M. Chakraborty, S.K. Bhattacharya, B. Show, A. Sarkar, P. Bera, H. Kim, M.M. Seikh and A. Gayen, *J. Rare Earths*, **40**, 725 (2022); <https://doi.org/10.1016/j.jre.2021.04.013>
2. M. Chalaris, D.A. Gkika, A.K. Tolkou, and G.Z. Kyzas, *Environ. Sci. Pollut. Res.*, **30**, 119627 (2023); <https://doi.org/10.1007/s11356-023-30891-0>
3. Y. Shi, J. Ma, Y. Chen, Y. Qian, B. Xu, W. Chu and D. An, *Sci. Total Environ.*, **804**, 150024 (2022); <https://doi.org/10.1016/j.scitotenv.2021.150024>
4. N. Alfryyan, I. Boukhris, S. Parveen, K.S. Albarkaty, Z. Alrowaili, M. Al-Buriah, K. Chaudhary, I. Shakir and M.F. Warsi, *Results Phys.*, **55**, 107142 (2023); <https://doi.org/10.1016/j.rinp.2023.107142>
5. E.H. Khader, T.J. Mohammed, N. Mirghaffari, A.D. Salman, T. Juzsakova and T.A. Abdullah, *Clean Technol. Environ. Policy*, **24**, 713 (2022); <https://doi.org/10.1007/s10098-021-02159-z>
6. M. Anwar, K.S. Alghamdi, S. Zulfiqar, M.F. Warsi, M. Waqas and M. Hasan, *Opt. Mater.*, **135**, 113336 (2023); <https://doi.org/10.1016/j.optmat.2022.113336>
7. M. Samy, K. Mensah, E.M. El-Fakharany, M. Elkady and H. Shokry, *Environ. Res.*, **223**, 115460 (2023); <https://doi.org/10.1016/j.envres.2023.115460>
8. K. Mensah, H. Mahmoud, M. Fujii, M. Samy and H. Shokry, *Biomass Convers. Biorefin.*, **45**, 102512 (2022); <https://doi.org/10.1016/j.jwpe.2021.102512>
9. E. Salama, M. Samy, H. Shokry, G. El-Subruiti, A. El-Sharkawy, H. Hamad and M. Elkady, *Sci. Rep.*, **12**, 22443 (2022); <https://doi.org/10.1038/s41598-022-26612-1>
10. M. Samy, M. Elkady, A. Kamal, N. Ellessawy, S. Zaki and M. Eltarahony, *Sustainability*, **14**, 14188 (2022); <https://doi.org/10.3390/su142114188>
11. K. Mensah, M. Samy, H. Mahmoud, M. Fujii and H. Shokry, *Int. J. Environ. Sci. Technol.*, **20**, 9717 (2023); <https://doi.org/10.1007/s13762-022-04646-2>
12. Z. Shen, Y. Zhou, Y. Guo, J. Zhao, J. Song, Y. Xie, Y. Ling and W. Zhang, *Chin. Chem. Lett.*, **32**, 2524 (2021); <https://doi.org/10.1016/j.ccl.2021.01.044>
13. F.M.A. Alzahrani, M. Anwar, M.F. Warsi, U. Younis, W. Adan, Z. Alrowaili, M. Al-Buriah and K. Chaudhary, *Mater. Chem. Phys.*, **315**, 129008 (2024); <https://doi.org/10.1016/j.matchemphys.2024.129008>
14. Y. Wang, J. Li, S. Chen, Y. Xie, Y. Ma, Y. Luo, J. Huang, Y. Ling, J. Ye, Y. Liang and J. Du, *J. Alloys Compd.*, **924**, 166569 (2022); <https://doi.org/10.1016/j.jallcom.2022.166569>
15. M. Samy, M.G. Ibrahim, M. Gar Alalm, M. Fujii, K.E. Diab and M. ElKady, *Chem. Eng. J.*, **395**, 124974 (2020); <https://doi.org/10.1016/j.cej.2020.124974>
16. K. Lakshmi, K. Kadirvelu and P.S. Mohan, *J. Chem. Technol. Biotechnol.*, **94**, 3190 (2019); <https://doi.org/10.1002/jctb.6126>
17. M. Samy, K. Mensah and M. Gar Alalm, *J. Water Process Eng.*, **49**, 103151 (2022); <https://doi.org/10.1016/j.jwpe.2022.103151>
18. A.A. Oun, S. Shankar and J.W. Rhim, *Crit. Rev. Food Sci. Nutr.*, **60**, 435 (2020); <https://doi.org/10.1080/10408398.2018.1536966>
19. S. Akgol, F. Ulucan-Karnak, C.I. Kuru and K. Kus, *Biotechnol. Bioeng.*, **118**, 2906 (2021); <https://doi.org/10.1002/bit.27843>
20. X. Zhou, C. Ding, C. Cheng, S. Liu, G. Duan, W. Xu, K. Liu and H. Hou, *Eur. Polym. J.*, **141**, 110083 (2020); <https://doi.org/10.1016/j.eurpolymj.2020.110083>
21. R. Jbeli, M. Lahmar, C. Bilel, F. Saadallah, H. Ouzari, M. Bouaïcha and M. Amlouk, *Optik*, **242**, 166837 (2021); <https://doi.org/10.1016/j.ijleo.2021.166837>
22. Z.N. Kayani, B. Amir, S. Riaz and S. Naseem, *Opt. Mater.*, **109**, 110287 (2020); <https://doi.org/10.1016/j.optmat.2020.110287>
23. C.R. Michel and A.H. Martinez-Preciado, *Sens. Actuators B Chem.*, **208**, 355 (2015); <https://doi.org/10.1016/j.snb.2014.11.034>
24. X. Ding, Y. Liu, L. Gao and L. Guo, *J. Alloys Compd.*, **425**, 318 (2006); <https://doi.org/10.1016/j.jallcom.2006.01.030>
25. K.B. Jinesh, V.A.T. Dam, J. Swerts, C. De Nooijer, S. Van Elshocht, S.H. Brongersma and M. Crego-Calama, *Sens. Actuators B Chem.*, **156**, 276 (2011); <https://doi.org/10.1016/j.snb.2011.04.033>
26. K. Krishna, K.S. Harisha, R. Neelakandan and Y. Sangappa, *Mater. Today Proc.*, **42**, 515 (2021); <https://doi.org/10.1016/j.matpr.2020.10.481>
27. M. Mylarappa, S. Chandruvasan, K.S. Harisha and K.N. Shravana Kumara, *Kuwait J. Sci.*, **51**, 100145 (2024); <https://doi.org/10.1016/j.kjs.2023.10.012>
28. M. Ghiasi and A. Malekzadeh, *Superlattices Microstruct.*, **77**, 295 (2015); <https://doi.org/10.1016/j.spmi.2014.09.027>
29. C. Kumari, P. Sharma, S.C. Katyal, M. Tanwar, P. Bamola, H. Sharma, R. Kumar and S. Chhoker, *Results Surf. Interfaces*, **9**, 100088 (2022); <https://doi.org/10.1016/j.rsufi.2022.100088>
30. Y. Li, L. Xue, L. Fan and Y. Yan, *J. Alloys Compd.*, **478**, 493 (2009); <https://doi.org/10.1016/j.jallcom.2008.11.068>
31. M.A. Marjehgal, A. Sedghi and S. Baghshahi, *J. Alloys Compd.*, **968**, 171765 (2023); <https://doi.org/10.1016/j.jallcom.2023.171765>
32. K. Wang, Y. Wu, H. Li, M. Li, F. Guan and H. Fan, *J. Inorg. Biochem.*, **141**, 36 (2014); <https://doi.org/10.1016/j.jinorgbio.2014.08.009>
33. S. Karthikeyan, K. Dhanakodi, S. Surendhiran, K. Jagan, N. Lenin, L. Dhatchinamurthy and A. Rajamanickam, *J. Mater. Sci. Mater. Electron.*, **34**, 1157 (2023); <https://doi.org/10.1007/s10854-023-10561-0>
34. Y. Xie, J. Wu, C. Sun, Y. Ling, S. Li, X. Li, J. Zhao and K. Yang, *Mater. Chem. Phys.*, **246**, 122846 (2020); <https://doi.org/10.1016/j.matchemphys.2020.122846>
35. K. Chaudhary, S. Zulfiqar, H. Somaily, M. Aadil, M.F. Warsi and M. Shahid, *Electrochim. Acta*, **431**, 141103 (2022); <https://doi.org/10.1016/j.electacta.2022.141103>
36. S. Chandruvasan, M. Mylarappa, S. Kantharaju and S. Rekha, *ECs Transitions*, **107**, 269 (2022); <https://doi.org/10.1149/10701.0269ecst>
37. V. Pathak, P. Lad, A.B. Thakkar, P. Thakor, M.P. Deshpande and S. Pandya, *Results Surf. Interfaces*, **11**, 100111 (2023); <https://doi.org/10.1016/j.rsufi.2023.100111>
38. W. Tang, H. Ye, Y. Xie, P. Chen, L. Luo and Y. Zhang, *Chem. Eng. J.*, **478**, 147350 (2023); <https://doi.org/10.1016/j.cej.2023.147350>